Nucleotide-Induced Conformational Changes in the *Saccharomyces cerevisiae* SR Protein Kinase, Sky1p, Revealed by X-ray Crystallography†

Brad Nolen,‡ Jacky Ngo,‡ Sutapa Chakrabarti,‡ Don Vu,‡ Joseph A. Adams,§ and Gourisankar Ghosh*,‡

Department of Chemistry and Biochemistry and Department of Pharmacology, University of California, San Diego, La Jolla, California 92093

Received March 24, 2003; Revised Manuscript Received May 20, 2003

ABSTRACT: Conformational changes are thought to play a key role in the function of active protein kinases, although little is known about how these changes relate to the mechanism of phosphorylation. Here we present four high-resolution structures of a single crystal form of Sky1p, a constitutively active serine kinase implicated in yeast RNA processing, each in a different state of nucleotide binding. By comparing the apoenzyme structure to the ADP- and ATP-bound Sky1p structures, we have revealed conformational changes caused by ATP binding or conversion from nucleotide reactant to product. Rotation of the small lobe of the kinase closes the cleft upon binding, allowing the nucleotide to interact with residues from both lobes of the kinase, although some interactions thought to be important for phosphotransfer are missing in the ATP-containing structure. In the apoenzyme, a kinase-conserved phosphate-anchoring loop is in a twisted conformation that is incompatible with ADP and ATP binding, providing a potential mechanism for facilitating ADP release in Sky1p. The nonhydrolyzable ATP analogue AMP−PNP binds in a unique mode that fails to induce lobe closure. This observation, along with comparisons between the two independent molecules in the asymmetric unit of each structure, has provided new molecular details about how the nucleotide binds and induces closure. Finally, we have used mutational analysis to establish the importance of a glycine within the linker that connects the two lobes of Sky1p.

The SR protein kinases (SRPKs)[1] are serine-specific kinases that phosphorylate SR proteins, a class of essential splicing factors (*1*, *2*). Phosphorylation of SR proteins affects multiple aspects of RNA processing, including constitutive and alternative splicing and mRNA export (*3*−*7*). SRPKs phosphorylate SR proteins on multiple serines within their RS domains, protein−protein interaction modules characterized by stretches of consecutive alternating serine and arginine residues (*8*, *9*). SRPKs also phosphorylate RS repeat-containing proteins with no direct links to RNA processing, including the lamin B receptor, phosphoprotamine 1, and the hepatitis B virus core protein (*10*−*12*). Indeed, the involvement of SRPKs in diverse processes is becoming clear. Chromatin condensation, chromosome segregation, ion homeostasis in yeast, and sensitivity to tumor drugs involve SRPKs, although in most cases it is not clear if the involvement is direct or caused by effects on RNA processing (*13*−*16*).

The previously reported structure of the apoenzyme form of an active, truncated Sky1p revealed how this *Saccharomyces cerevisiae* SRPK remains active without requiring activation loop phosphorylation (*17*). The two lobes of the Sky1p structure are in an intermediate conformation relative to open and closed conformations seen in other protein kinase catalytic domain structures. The collection of kinase structures, in fact, shows that the kinase core can adopt many different conformations because of flexibility in both the orientation of the two lobes and in loops emanating from each lobe (*18*). Opening and closing of the lobes in protein kinases was first observed in the comparison of a ternary (enzyme/ATP/inhibitor peptide) and binary (enzyme/iodinated inhibitor peptide) crystal structure of the catalytic subunit of cAMP-dependent protein kinase (PKA) (*19*). It was postulated that these conformational changes accommodate nucleotide binding and may be a necessary part of the catalytic cycle. This suggested that active kinases must be able to adopt a number of conformations in solution, any of which might be captured in crystal structures. Since the nucleotide is tightly wedged into the catalytic cleft in the PKA ternary structure, ATP association or ADP dissociation is likely to require opening of the cleft. Furthermore, contacts between the phosphates and conserved residues from both lobes, which are thought to be essential for catalysis, can only be made when the cleft is closed.

Pre-steady-state kinetic work suggests that slow conformational changes are an integral part of the catalytic mechanism of PKA (*20*, *21*). These conclusions have recently been extended to two tyrosine kinases, Csk and Her-2,

† This work was supported by an American Heart Association doctoral training fellowship (0110037Y) to B. N.

* To whom correspondence should be addressed. Phone: (858) 822-0469. Fax: (858) 534-7042. E-mail: gghosh@ucsd.edu.

‡ Department of Chemistry and Biochemistry.

§ Department of Pharmacology.

[1] Abbreviations: AMP−PNP, 5′-adenylylimidodiphosphate; CDK2, cyclin-dependent kinase 2; CK1, casein kinase 1; CNS, crystallography and NMR system; Csk, C-terminal Src kinase; ERK2, extracellular signal-regulated kinase 2; FRET, fluorescence resonance energy transfer; MAPK, mitogen-activated protein kinase, PKA, cAMP-dependent protein kinase; PKI, protein kinase inhibitor protein; Sky1p, SR-protein kinase in yeast; Sky1pΔNS, Sky1p lacking the spacer inset and 127 amino acids from the N-terminus; SRPK, SR protein kinase.

10.1021/bi0344331 CCC: $25.00
Published on Web 07/29/2003

indicating that slow structural changes may be a general feature of the catalytic pathway in this enzyme family (*22*, *23*). Establishing the connection between these kinetic findings and structural data is important for understanding kinase function on a molecular level. Deuterium-exchange methods have demonstrated differences in solvent accessibility in different states of nucleotide binding in PKA and the C-terminal Src kinase (Csk) (*24*, *25*). Fluorescence resonance energy transfer (FRET) experiments on PKA have demonstrated that in solution, the lobes are, on average, more closed when the nucleotide is bound (*26*). These solution-based studies indicate that both local and distal structural changes are associated with nucleotide binding. However, these methods have not yet been able to detect conformational changes on the time scale of phosphotransfer.

Crystallographic data provides a powerful method for investigating ligand binding. However, it can be difficult to define the origins of conformational changes observed in ligand-bound crystal structures because crystal packing forces can affect conformation. Crystal growth, in fact, can select certain conformations of dynamic molecules distributed in solution. The structure of Csk, for example, includes two very different conformations in the asymmetric unit (*27*). One is described as active and the other as inactive, although the molecule probably rapidly interchanges between both conformations in solution.

Here we report a new apoenzyme structure of an active fragment of Sky1p (the construct Sky1pΔNS includes the entire kinase domain but lacks 137 amino acids from the N′ terminus and the spacer region that bifurcates the kinase domain), along with three nucleotide-containing (ATP, ADP, and AMP−PNP) structures. Because each structure maintains the same packing arrangement, we can discern changes due solely to nucleotide binding. This information has provided insight into the relationship between nucleotide binding and conformation in the SRPK family in particular and the protein kinase superfamily in general.

MATERIALS AND METHODS

Cloning, Expression, and Purification. Sky1ΔNS (residues 138−304 and 538−742) was expressed, purified, and crystallized as previously described (*17*). The Sky1ΔNS-(G250A) mutant was generated by one-step PCR amplification using Sky1ΔNS in pET15b as a template and the primers 5′-AgCCAgTAAgTTCTCggCTAgCACTTC AAATACCAT-AAC-3′ and 5′-gTTATggTATTTgAAgTgCTAgCCgAgAA-CTTACTg gCT-3′. After digestion with DpnI (NEB), the nicked product was transformed into DH5α *Escherichia coli*. Plasmids isolated from transformants were analyzed by restriction analysis and sequencing to verify the presence of the mutation. Sky1ΔNS(G250A) was expressed and purified using the same procedure as for the wild type. Protein concentrations was determined by the von Hippel method (*28*).

Npl3p in pET15b was transformed into BL21(DE3) plays (Invitrogen) *E. coli* cells. Cells were grown in 2 L of LB broth containing 200 μg/mL of ampicillin to an OD_{600} of 0.8. Protein expression was induced with 0.2 mM of isopropylthiogalactoside and carried out at 22 °C for 12 h. Cells were resuspended in 100 mL of buffer containing 20 mM of Tris-HCl (pH 7.5), 5 mM of imidazole, 500 mM of NaCl, 10% glycerin, 0.5 mM of phenylmethylsulfonyl fluoride, and 0.5 mL of protease inhibitor cocktail (Sigma) and lysed by sonication. The crude lysate was spun at 15000*g* for 30 min. The soluble fraction was loaded onto a Ni−NTA column, washed with lysis buffer containing 40 mM of imidazole, and eluted with the same buffer containing 250 mM of imidazole. The eluent was diluted to an NaCl concentration of 100 mM, loaded on to a Q-sepharose fast flow column, and washed with buffer containing 20 mM of Tris-HCl (pH 7.5), 100 mM of NaCl, 1 mM of DTT, 0.5 mM of EDTA, and 10% glycerol. The protein eluted from a 100−500 mM NaCl gradient at about 250 mM. NaCl was added to pooled fractions to bring the salt to 1 M. After concentration in a centriprep 30 (Millipore), the protein was loaded onto a Superdex 200 size-exclusion column (Amersham Biosciences). Pooled fractions were concentrated and flash frozen.

Kinase Assays. Reactions (20 μL) were initiated by adding Sky1ΔNS or Sky1ΔNS(G250A) to a mix to give a final reaction concentration of 0.05 μM of kinase, 20 μM of Npl3p, 1 mM of ATP, 50 mM of MOPS (pH 7.2), 50 mM of NaCl, 0.01% Brij (polyoxyethyleneglycol dodecyl ether), 5 mM of MgCl2, 50 mM of NaCl, 1mM of DTT, and 100 μCi/μmol γ-^{32}P−ATP. The substrate for the reaction, Npl3p, is a *S. cerevisiae* protein with a single C-terminal Sky1p phosphorylation site. Phosphorylation was carried out at 22 °C and stopped by adding SDS gel-loading buffer. Reactions were boiled and run on 10% SDS-PAGE gels. Gels were dried and exposed to a phosphorimaging screen for quantitation.

Solving the Nucleotide-Containing Structures. We reported previously that the apoenzyme form of Sky1p crystallizes in 1.5 M of ammonium sulfate, 15% ethylene glycol, and 10 mM of sodium acetate (pH 4.5) (*17*). Attempts to cocrystallize both ATP−Mg^{2+} and ADP−Mg^{2+} with Sky1p in these conditions yielded no electron density for the ligands.

Sulfates of crystallization occupy both the substrate-binding groove and the active-site cleft in the apoenzyme (1HOW) structure. We reasoned that either the bound sulfates or nonspecific electrostatic shielding due to the high ammonium sulfate concentration may prevent nucleotide binding. Hence, we exchanged the ammonium sulfate for 35% PEG 400 by dialysis. Crystals could be dialyzed into 35% PEG 400 and either 15% ethylene glycol or 100 mM of sodium acetate without cracking. Dialyzed crystals were then soaked for 24 h in stabilization buffer containing 10 mM of nucleotide plus 10 mM of $MgCl_2$.

The crystals exchanged into 35% PEG 400 and 15% ethylene glycol had the same space group as the ammonium sulfate-containing apo-form Sky1p structure (1HOW) previously reported ($C222_1$). However, when the crystals were dialyzed into 35% PEG 400 and 100 mM sodium acetate, they indexed as $P2_12_12_1$ with the same (approximate) unit cell lengths as the $C222_1$ crystals. Because we were able to determine the structure of the apoenzyme and each nucleotide-bound (ADP, ATP, and AMP−PMP) form of Sky1p in the $P2_12_12_1$ space group, but not in the $C222_1$ space group, the $P2_12_12_1$ structures will be the focus of this paper.

The $P2_12_12_1$ crystals contain two molecules per asymmetric unit, whereas the $C222_1$ crystals contain only one. To generate a starting model for the solution of the $P2_12_12_1$ structures, we used the previously reported Sky1p structure;

Table 1: Crystallographic Data and Refinement Statistics

	APO	ATP	ADP	AMP−PNP
		Data Collection[a]		
space group	$P2_12_12_1$	$P2_12_12_1$	$P2_12_12_1$	$P2_12_12_1$
unit cell dimensions				
a (Å)	72.99	71.82	71.58	72.41
b (Å)	88.70	88.69	88.65	88.95
c (Å)	135.6	133.5	133.8	134.8
resolution max (Å)	2.35	2.30	2.05	2.10
total observations	198 041	178 325	298 198	280 589
unique observations	34 172	33 170	50 520	49 644
completeness (%)	91.6/85.6	86.0/83.3	98.1	96.5
R_{sym}(%)[b]	6.7/63.6	8.1/54.4	6.8/41.1	8.5/46.7
I/s	10.3/2.39	8.8/4.2	21.1/3.2	14.9/2.3
		Model Refinement		
reflections	28 641	29 551	37 868	41 455
R_{cryst}[c]	22.1	20.39	21.02	22.01
R_{free}[d]	25.9	25.63	24.46	26.01
bond angle rmsd (deg)	1.33	1.27	1.26	1.27
bond length rmsd (Å)	0.007	0.007	0.006	0.007
avg B factor (Å^2)				
main chain	36.2	32.9	25.1	28.9
side chain	38.0	35.0	27.5	31.5
nucelotide (molA)	−	50.1	29.5	34.6
nucelotide (molB)[e]	−	74.9	46.9	38.6

[a] All data collected at SBC 19ID at the Advanced Photon Souce and processed using HKL2000 (Otwinowski, Z., and Minor, W. (1997) *Methods Enzymol. 276*, 307−336). [b] $R_{sym} = \sum |I - \langle I \rangle| / \sum I$. [c] $R_{cryst} = ||F_{obs}| - |F_{calc}||/|F_{obs}|$. [d] $R_{free} = ||F_{obs}| - |F_{calc}||/|F_{obs}|$ for the 5% of the data not used in the refinement. [e] Because of poor density, only the adenine ring was modeled into the active site of molecule B of the ATP-soaked crystals, and adenosine was modeled into the active site of molecule B in the ADP-soaked crystals.

by translating the origin of the unit cell and rotating the coordinates about the twofold symmetry axis that distinguishes the $C222_1$ space group from the $P2_12_12_1$ space group, we generated the second molecule in the asymmetric unit.

The models were refined using CNS (*29*). The two lobes of the kinase were allowed to move independently in the first round of rigid body refinement. Subsequent Powell minimization yielded models with initial R factors below 34% for each of the $P2_12_12_1$ structures. $F_o - F_c$ difference electron-density maps generated with phases from these models showed strong density for the nucleotide in the active site of molecule A of each structure. The active site of molecule B in the ADP and ATP structures showed weaker and incomplete density; only during later stages of refinement were adenine and adenosine added, respectively. The results of iterative rounds of rebuilding followed by minimization are tabulated in Table 1. A $2F_o - F_c$ electron-density map with nucleotides omitted from the phase calculation was generated for each nucleotide-containing structure (Figure 1).

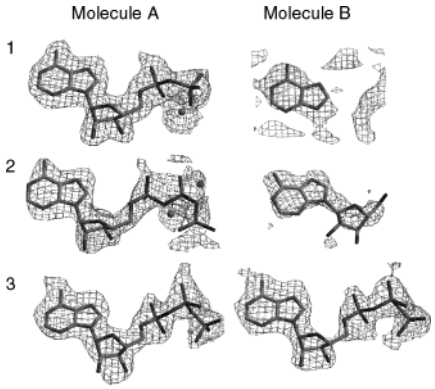

FIGURE 1: Simulated annealing omit map showing electron density of nucleotides. Nucleotides were omitted from the phase calculations in the ADP-, ATP-, and AMP−PNP-containing structures (rows 1, 2, and 3, respectively) and are shown here with the calculated 1.0σ $2F_o - F_c$ omit map electron density. Density is consistently stronger for nucleotides in molecule A. In molecule B, only AMP−PNP showed complete density for the entire nucleotide. This figure was made with Xtalview and Raster3d (*52*, *53*).

RESULTS AND DISCUSSION

Overall Conformation. The α carbons from the large lobe of crystallographically equivalent molecules were overlaid to examine nucleotide-induced conformational changes. A comparison of each molecule in the first position, hereafter referred to as molecule A, revealed that the small lobe of both the ADP and ATP structures rotates 7.0 and 5.1°, respectively, relative to the new apoenzyme structure. Rotation occurs about an axis that runs diagonally through the back of the active-site cleft, moving strands β0 to β5 and the N-terminal end of the αC helix forward on the Z axis and down on the Y axis so that the active-site cleft becomes deeper and narrower (Figure 2).

In the second position (molecule B of each structure), the small lobe rotates in the opposite direction about the hinge, and the active-site cleft opens, becoming shallower and wider. The magnitude of this movement is inversely correlated to how much molecule A closes. For example, molecule A is most closed in the ADP-containing structure, but molecule B in the same structure is more open than molecule B in any of the other structures (Figure 2). This suggests that to maintain crystal contacts, closure of molecule A must be accompanied by the opening of molecule B. In addition, while molecule A is free to close, crystal packing forces prevent molecule B from closing. The mechanistic implications of these observations will be discussed later.

For each structure, the electron density for molecule A is discontinuous in the αF/αG loop and within the MAPK

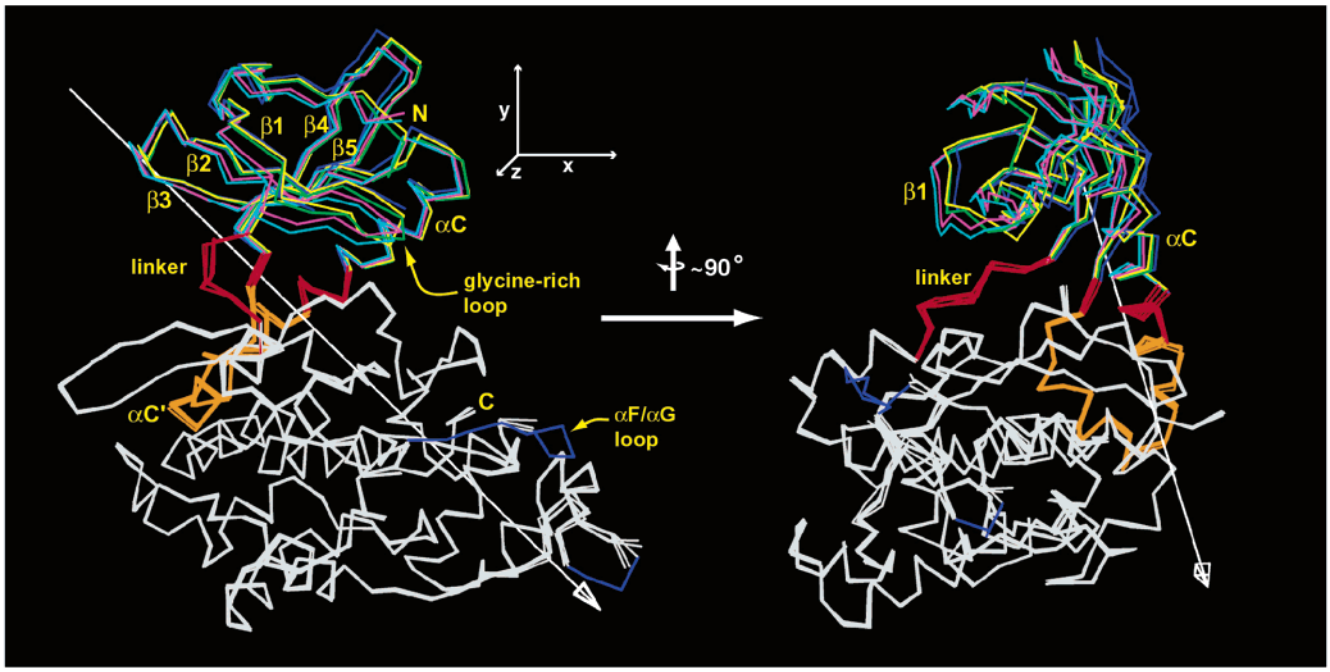

FIGURE 2: Large lobe overlay. (a) Binding of nucleotide induces conformational changes in Sky1p, including a rotation and translation of a portion of the small lobe about a screw axis that runs diagonally through the back of the active site (long white arrow). The large lobes of molecule A from each of the four structures and molecule B from the ADP-soaked crystal were overlaid using the program O (*54*). Regions used for the superposition are colored light gray. The portion of the small lobe which undergoes rigid body movement is colored as follows: Molecule A: apoenzmye, yellow; AMP−PNP, green; ATP, magenta; ADP, cyan. Molecule B: ADP, blue (note that part of the glycine-rich loop is not modeled because of missing electron density). Residues 604−615 (αF/αG loop) and 643−649 (MAPK insert) are colored blue and were disordered in molecule A, but ordered in molecule B of each structure. The C-terminal end of helix αC and the αC′ helix (orange) superpose well, even though they were not explicitly overlaid and are functionally part of the large lobe. Movement of the lobes was characterized using the program Dyndom (*55*). Residues that serve as hinges for the movement are colored red. An approximately 90° rotation about the *y* axis in (a) produces the view in panel (b). This figure was made with Molscript and Raster3d (*56*).

insert. In molecule B of each structure, the αF/αG loop has high B factors but is ordered, forming a short flap that contacts a symmetry-related molecule. This loop, an integral part of the substrate-binding groove, is variable in length and sequence among protein kinases and is often disordered or has high B factors in X-ray crystal structures (*30*−*32*). In protein kinase A, the αF/αG loop interacts with the N-terminal region of the PKI inhibitor peptide, which confers high-affinity binding (*33*). The αF/αG loop of Sky1p may play a similar role in interacting with protein substrates by becoming more rigid upon binding. A short portion of the MAPK insert that is disordered in molecule A is also ordered in molecule B of each structure (Figure 1).

Clear density was observed for the nucleotides in molecule A. In contrast, we were only able to model adenine and adenosine into the weak nucleotide density observed in molecule B in the ADP- and ATP-containing structures, respectively. Therefore, the next section will focus on specific differences between molecule A of the apoenzyme, ADP-, and ATP-containing structures.

ADP vs ATP Binding in Molecule A. Adenine Ring. The back of the ATP-binding cleft forms a hydrophobic pocket for the adenine ring. In the nucleotide-containing protein kinase structures solved to date, three highly conserved residues form the primary set of van der Waals interactions with the ring. In Sky1p, these residues are Val172, Ala185, and Leu301. Val172 and Ala184 from β2 and β3 in the small lobe, respectively, form the top of the pocket, and Leu301, from β7 in the large lobe, occupies the most central position in the hydrophobic lining at the bottom of the pocket (Figure 3).

In both the ADP and ATP structures, the width of the cleft decreases by more than 1 Å relative to the apoenzyme, creating a tighter pocket. In the ADP structure, greater rotation of the small lobe and an independent downward movement of the glycine-rich loop further closes the cleft relative to the ATP structure. These differences are amplified in regions further from the axis of rotation. Consequently, although the back of the ring (atoms N1, C2, C3, and C6) fits snugly in both structures, the distance between Val172 CG2 at the top and front of the hydrophobic pocket and Leu301 CD2 on the bottom is 0.45 Å greater in the ATP-containing structure.

Ribose. In both the ADP and the ATP-containing structures, the ribose ring exhibits a 3′-endo pucker. The 2′- and 3′-hydroxyl oxygens of ADP hydrogen bond to the side chain of Asn252, a residue immediately C-terminal to the linker polypeptide that connects the two lobes (Figure 3). The 3′-OH of ADP is also hydrogen-bonded to the backbone carbonyl oxygen of a S/T kinase-conserved residue from the catalytic loop, Glu298. The ribose moiety from ATP occupies a slightly more open cleft compared to ADP and is further from the bottom of the cleft. Hence, only one hydrogen bond, between the 3′-OH and Asn252, anchors the ATP ribose to the large lobe.

Although the hydrogen-bonding potential of the residue equivalent to Asn252 is conserved in most protein kinases, its exact role in catalysis is still uncertain (*34*). Dissection

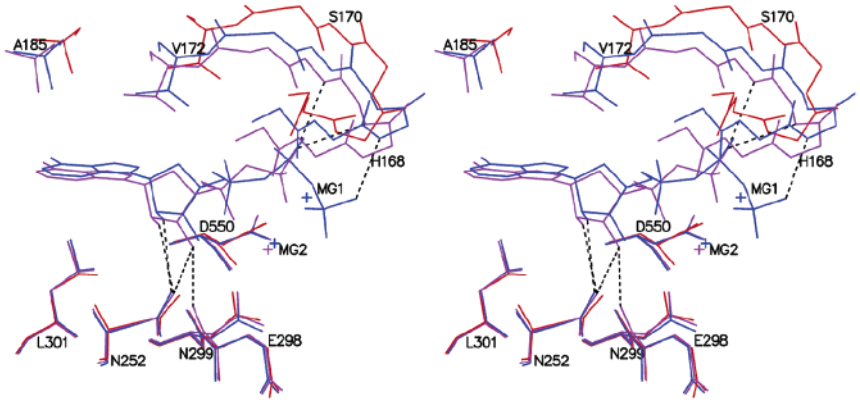

FIGURE 3: Stereoview of nucleotide binding in molecule A. Coordinates from the large lobe overlays of molecule A from the apoenzyme (red), ATP (blue), and ADP-containing (violet) structures were used to make this figure. The cleft is most open in the apoenzyme structure and is most closed in when ADP is bound (purple). The ATP-filled cleft is slightly more open than the ADP-containing cleft and makes fewer contacts to the nucleotide. Two magnesium ions position the phosphates of ATP. Only one magnesium (Mg2) is visible in the ADP structure, suggesting that Mg1 dissociates immediately after phosphotransfer. The glycine-rich loop of the apoenzyme structure adopts a twisted conformation which will be described in a separate section.

of its function is complicated by its critical location; in crystal structures of PKA and phosphorylase kinase, it contacts both the ribose and the substrate peptide (*32*, *33*). In PKA this residue (Glu127) is sensitive to mutation because of its role in contacting the P-3 arginine in the substrate (*35*). The hydrogen bonding between Glu127 and the furanose hydroxyls observed in the PKA crystal structure cannot be disrupted by mutation without abolishing peptide binding. However, in the structure of active cyclin-dependent kinase 2 with bound substrate, the peptide does not contact the residue equivalent to Asn252 in Sky1p (*36*). Because modeling studies have indicated that Sky1p is likely to have a peptide-binding mode similar to that of CDK2, we predict that Asn252 in Sky1p does not play a role in binding peptide or protein substrates and serves only as an anchor for the ribose (*17*).

It is uncertain whether the ribose-anchoring function of Asn252 increases the affinity for ATP or if hydrogen bonding to the ribose promotes lobe closure. The apparent plasticity of the hydrogen bonds to the ribose hydroxyls in our structures suggests that the latter may be more important. In support of this, the crystal structure of the insulin-like growth factor receptor provides another example of an active protein kinase with bound ATP in which the ribose is not anchored because of incomplete closure of the lobes (*37*). In the crystal structures of PKA or CDK2 with bound transition-state mimics, which represent a snapshot of these enzymes during phosphotransfer, the ribose is anchored by the Asn252 equivalent (*38*, *39*). This suggests that furanose anchoring may be a characteristic of the stabilized transition state. We propose that hydrogen bonding to the ribose is a conserved feature that may increase the affinity for ATP and favors closing of the lobes, but the furanose hydroxyls are not anchored in each of the conformations adopted by an active kinase.

Phosphates. The glycine-rich loop of protein kinases plays a role in binding the nucleotide and positioning the phosphates for phosphoryl transfer (*40*, *41*). Multiple conformations of the loop have been observed in protein kinase crystal structures, and B factors of the loop are generally higher than those in the rest of the molecule. This observation holds true for Sky1p: in both the apoenzyme and nucleotide-bound structures, the loop has B actors about 20 Å^2 higher than the average for each structure.

The hydrogen bond between the backbone amide of His168 and the γ phosphate is the only hydrogen bond between the glycine-rich loop and the phosphates in the ATP-bound structure (Figure 3). This interaction occurs in other protein kinase structures and is thought to be the most critical in positioning the γ phosphate. A kinase-conserved glycine (Gly167) allows the backbone of His168 to adopt the proper geometry to hydrogen bond to the phosphate. In PKA, mutation of the glycine equivalent to Gly167 disrupts this hydrogen bond and has severe kinetic consequences (*42*, *43*). However, it is not clear if hydrogen bonding between the loop and the phosphates is a general requirement for phosphotransfer. In both phosphorylase kinase and CDK2, for example, the glycine-rich loop is turned inward slightly, although both structures represent active forms of the kinase with ATP analogue and substrate peptide bound (*32*, *44*). In these structures, the phosphates are not nested directly underneath the bottom of the loop but sit beneath the edge of the loop, which provides no hydrogen bond donors. In CDK2, interactions with the loop are absent even in the transition-state analogue structure, which provides a snapshot of the kinase during phosphotransfer (*38*).

In the ADP-containing structure, we observed greater lobe rotation and a downward movement of the entire glycine-rich loop, which creates a tighter fit for the product nucleotide and more hydrogen bonding between the phosphates and the kinase (Figure 3). This may explain the lower average B factor for ADP (29.5 Å^2) compared to ATP (50.1 Å^2) in the two structrures. The β phosphate of ADP is repositioned relative to the ATP structure and makes hydrogen bonds to the backbone amides of both Phe169 and Ser170 from the tip of the glycine-rich loop. Lys187, a kinase-conserved residue from β3, is thought to bind and position the α and β phosphates. This residue makes 3.19 and 3.30 Å hydrogen bonds to the α and β phosphate oxygens in the ADP-containing structure, respectively. In the ATP-containing structure, Lys187 is within hydrogen-bonding distance of the α and β phosphates, but the phosphate oxygens are positioned too high in the active-site cleft to accept the hydrogen.

Magnesium. Two magnesium ions are bound in the active site of the ATP-containing structure. One magnesium (Mg1) is chelated by both side-chain oxygens of Asp550, and another (Mg2) is chelated by Asp550 from the Mg^{2+}-binding loop and Asn299 from the catalytic loop (Figure 3). Steady-state kinetic analysis of Sky1p has shown that binding of one magnesium is essential and binding of a second further enhances catalysis (*45*). Although order-of-addition experiments have not yet been performed, the lower B factor of Mg2 (44.4 Å^2) compared to Mg1 (58.2 Å^2) suggests that it may bind more tightly and, thus, could precede the binding of Mg1.

In the ATP structure, Mg1 is 2.09 Å away from the $\beta-\gamma$-bridging oxygen. Because of the position and torsion of the phosphates, Mg1 does not contact the nonbridging oxygens of the β and γ phosphates, as it does in many other protein kinase structures. Mg2, in contrast, contacts nonbridging oxygens on the α and γ phosphates; these interactions are typical for protein kinases with ATP or ATP analogues bound.

In the ADP structure, density is visible for Mg2 only. This magnesium remains bound to the α phosphate, and the lost interaction with the γ phosphate is replaced with a contact to the repositioned β phosphate.

In PKA, Mg1 binds tightly and is essential for catalysis (*46*). In comparison, Mg2 binds with lower affinity and decreases substrate turnover by stabilizing ADP, subsequently preventing release of this product. Interestingly, the structure of PKA with bound ADP and substrate peptide contains no magnesium, and the β phosphate exhibits poor electron density, suggesting that it is flexible (*47*). Finally, many active protein kinases with bound ATP or ATP analogues bind only one magnesium in the active site (*30*, *38*, *48*). In these kinases, the magnesium occupies the Mg2 site, suggesting that the affinity at this site may be higher than for the Mg1 site, as in Sky1p. Taken together, these results suggest that protein kinases exhibit different relative affinities at their magnesium-binding sites and that the exact role of the magnesium in individual steps of catalysis may vary depending on the kinase.

Mechanistic Implications. The intermediate conformation of the cleft and relatively few kinase−nucleotide interactions in the ATP structure offer a molecular basis for the high K_{ATP} observed for Sky1p (200 μM) (*45*). It is unclear, however, how the differences between the ATP- and ADP-containing structures play into the mechanism of catalysis. Although there is little data on conformational differences between ADP- and ATP-bound forms of protein kinases, FRET experiments on PKA indicated that the average distance between probes on the large and small lobes decreased significantly upon nucleotide binding and that the ADP-bound form had the shortest average distances (*26*). This is despite the fact that the lobe orientations in ADP-bound versus those in ATP-bound crystal structures of PKA are nearly identical. It is therefore possible that in PKA, both nucleotides favor complete closing, but in solution, a fully closed state is more often occupied when ADP is bound.

To more closely examine the mechanistic implications of the less complete closure in the Sky1p ATP-containing structure, we analyzed the positions of residues involved in catalysis. In the previously reported apoenzyme structure, we modeled a peptide derived from the Sky1p phosphorylation site in Npl3p into the peptide-binding groove of the Sky1p (*17*). When this modeled peptide is superposed onto the ATP-containing Sky1p structure, the distance between the P-site hydroxyl and the γ phosphorus atom is 4.07 Å, longer than expected to facilitate nucleophilic attack by the hydroxyl group. In the phosphorylase kinase and cyclin-dependent kinase structures containing ATP and substrate peptide, this distance is 3.6 and 3.7 Å, respectively (*32*, *36*). In the PKA and CDK2 structures with transition-state analogues bound, the distance (measured to the atom mimicking the γ phosphorus) shortens considerably (*38*, *39*).

Also affected by incomplete closure is the interaction between the γ phosphate and the side-chain amino group of Lys296, which are 5.92 Å apart in the Sky1p ATP-containing structure. This lysine, a residue from the catalytic loop which is conserved among S/T kinases, interacts with the γ phosphate in some nucleotide-containing complexes. This interaction has been hypothesized to help stabilize the transition state and may also help pull the equilibrium in favor of the closed state (*39*, *49*). Mutation of this residue in PKA leads to a 300-fold decrease in specific activity (*50*). As in Sky1p, the equivalent lysine is not within hydrogen-bonding distance of the γ phosphate in CDK2 structures containing ATP (*36*). However, in the crystal structure of CDK2 complexed with ADP and nitrate, the nitrate, which mimics the γ phosphate at the transition state, hydrogen bonds to the catalytic-loop lysine in only one of the two crystallographically related molecules (*38*). These observations suggest that transient contact may occur during catalysis but that the interaction is not always captured in crystal structures. Alternatively, if the effect of the lysine is largely electrostatic, direct contact may not be necessary. In either case, it is likely that in Sky1p, the γ phosphate would have to be closer than 5.92 Å for the lysine to have a significant stabilizing effect on the negatively charged transition state.

Considering that closing of the cleft allows the phosphates to contact these catalytic residues from the large lobe, it seems somewhat unintuitive that the ATP structure is more open than the ADP structure. We propose two explanations for this: (1) full closure might also be induced by peptide-binding or (2) a fully closed ATP-bound state is not a low-energy conformation, and it eludes crystallographic capture. Both of these possibilities highlight the fact that there is not one active conformation of a protein kinase but that a range of conformations are adopted during the catalysis.

AMP−PNP Binds without Inducing Conformational Changes. Although Sky1pΔNS crystals were soaked with the non-hydrolyzable ATP analogue AMP−PNP in the presence of 10 mM of magnesium chloride, no density for Mg^{2+} was observed. The nitrogen bridging the β and γ phosphate in the AMP−PMP molecule is close to the binding site for Mg1 and hydrogen bonds to the side-chain carboxyl of Asp550 (Figure 4A). ATP cannot make this interaction because the bridging oxygen lacks a donor hydrogen.

The phosphates of AMP−PNP are positioned under the loop in an orientation similar to that in ATP. However, the direct contact to Asp550 allows the AMP−PNP to bind further toward the back of the catalytic cleft (toward the Mg^{2+}-binding loop and helix αC) so that the conformational changes which pull the small lobe out and down to make the cleft narrower and deeper, as seen in the ADP and ATP structures, are not required for AMP−PNP binding (Figure

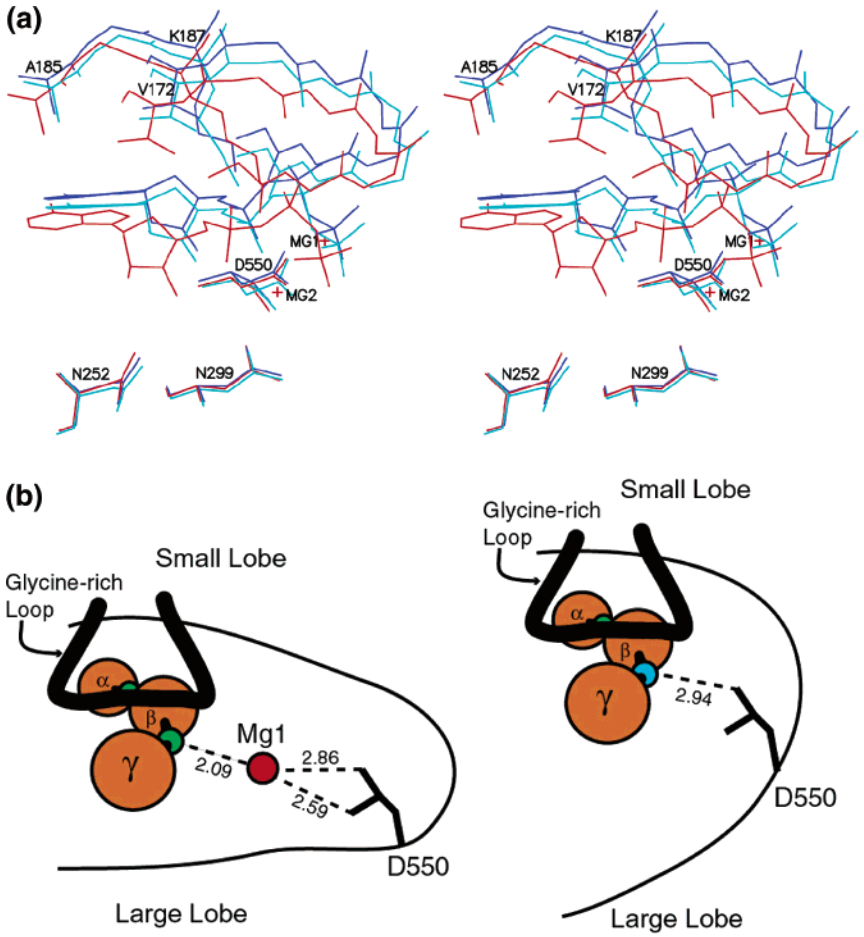

FIGURE 4: Mechanism of AMP−PNP binding. (a) Stereoview of AMP−PNP and ATP-containing active sites. AMP−PNP binds to the top of the open cleft in both molecule A (cyan) and molecule B (blue). Compared to molecule A of the ATP-containing structure (red), the AMP−PNP phosphates bind deeper in the pocket, making a direct contact with Asp550, a kinase-conserved residue which chelates both magnesiums in the ATP-containing structure. In contrast, no magnesium is observed in the active site when AMP−PNP is bound. (b) AMP−PNP binds to the open conformation. The phosphates of AMP−PNP contact Asp550 directly instead of through a magnesium, as in ATP. Therefore, closing of the lobe to create a deeper cleft is not necessary for the phosphates to interact with Asp550 while simultaneously interacting with the bottom of the glycine-rich loop. The left panel illustrates how positioning the phosphates of ATP underneath the loop requires a deeper (closed) cleft because of the interaction with magnesium. The bridging oxygens are colored green. The right panel illustrates how the hydrogen bond between the imido group of AMP−PNP and the side-chain carboxyl of Asp550 allows AMP−PNP to bind to a wide and shallow active-site cleft. The imido nitrogen, which bridges the β and γ phosphates, is colored cyan. Distances are in Å.

4B). Indeed, when we overlaid the large lobes of molecule A of the apoenzyme and AMP−PNP structure, we found that AMP−PNP did not induce lobe closure (Figure 1).

Molecule B and the Mechanism of Nucleotide Binding. As previously noted, the electron density for the nucleotides in molecule B of the ATP and ADP structures is weak and incomplete, and we were only able to model adenosine and adenine into the active sites, respectively. We attribute this to the fact that molecule B cannot close on the nucleotide without losing intermolecular contacts that are important for crystal packing. In support of this, we have observed that the $C222_1$ apoenzyme crystals, which contain one kinase molecule (in an open conformation) per asymmetric unit, stabilized in PEG 400 and ethylene glycol (instead of sodium acetate) crack when soaked with ADP. However, we observed strong electron density for the entire AMP−PNP molecule in B, even though the cleft is open (Figures 1 and 4). These observations suggest that for the ribose and phosphates of Mg−ADP and Mg−ATP to become ordered in the active site of Sky1p, they must hydrogen bond to the underside of the glycine-rich loop and simultaneously contact Asp550 through the bridging magnesium. To maintain this dual set of interactions, the kinase domain must assume a closed conformation.

The adenine ring in molecule B of the ADP- and ATP-soaked crystals makes van der Waals contacts to the aliphatic residues from the small lobe, which line the top of the hydrophobic pocket. However, the ring does not contact the hydrophobic residues from the bottom of the pocket. This phenomenon of "sticking to the roof" was also observed in the ATP-bound form of the insulin-like growth factor 1 receptor kinase and may be indicative of a common mode for nucleotide binding to the open catalytic cleft (*37*). In the case of Sky1p, the lack of electron density for the phosphates (and ribose) in molecule B suggests that the adenine ring binds first by wedging tightly against the linker at the back of the pocket and sticking to the roof. This interaction results in conformational changes that make the cleft deeper and tighter so that hydrophobic residues from both lobes tightly sandwich the adenine. The movement also positions the glycine-rich loop so that the phosphates can hydrogen bond to the bottom of the loop while the β and γ phosphates simultaneously bind to Asp550 in the Mg^{2+}-binding loop through the Mg1. We speculate that release of the nucleotide

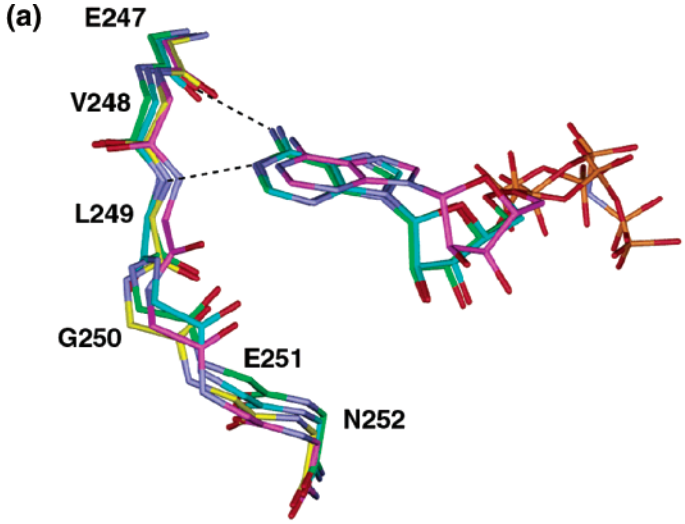

	E247		V248		L249	
	Φ	Ψ	Φ	Ψ	Φ	Ψ
APO	-74.7	151.5	-76.6	138.0	-148.4	96.9
ADP	-79.1	159.2	-78.5	129.6	-134.6	84.4
ATP	-92.2	151.1	-71.4	135.3	-124.6	-4.4
AMP-PNP	-78.2	155.3	-84.6	124.6	-114.6	160.6

	G250		E251		N252	
	Φ	Ψ	Φ	Ψ	Φ	Ψ
APO	37.0	-152.9	-121.9	162.5	-74.0	165.7
ADP	32.6	-142.2	-113.4	170.4	-82.8	168.6
ATP	101.4	-146.5	-96.4	157.6	-83.8	167.6
AMP-PNP	-65.5	-150.0	-77.1	165.4	-85.7	175.9

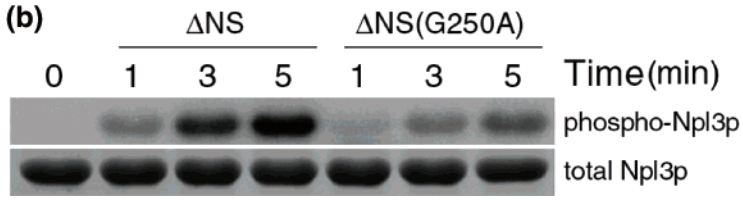

FIGURE 5: Conformation of the linker. (a) Residues in the linker region adopt different conformations dependent on the state of nucleotide binding. The Φ−Ψ angles of Leu249 and Gly250 change dramatically, indicating that this portion of the linker is flexible. The backbone conformation of molecule A of the AMP−PNP structure (magenta) causes the carbonyl of Leu249 to protrude into the active-site cleft, pushing the adenine ring higher in the pocket. The other structures (all molecule A) are colored as follows: ADP, green; ATP, blue; apoenzyme, yellow. In each of the nucleotide-containing structures, the N1 and N6 of the adenine ring hydrogen bond to the linker backbone. For simplicity, these bonds are only shown for the ADP structure in this figure. (b) Mutation of a glycine in the linker decreases the specific activity of Sky1pΔNS. Sky1pΔNS or Sky1pΔNS(G250A) (0.05 μM each) and 1 mM ATP were used to phosphorylate 20 μM Npl3p, a yeast substrate with a single Skly1p phosphorylation site. Reaction times were limited to keep the total amount of product turnover below 10%, as quantitated by phosphorimaging (top row). The bottom row shows a Coomassie stain of each of the time points.

occurs in the opposite manner, with the phosphates and ribose being released before the adenine ring.

Flexibility of the Linker. Lobe closure in Sky1p occurs by a hinge movement that involves bending at three points: the linker between the two lobes, the C-terminal portion of αC, and the loop between αC′ and β4 (Figure 2). The linker may be the most critical hinge point because it forms part of the ATP-binding pocket, making backbone-mediated hydrogen bonds to both N1 and N6 of the adenine ring.

Hinge bending occurs through changes in Φ−Ψ torsions, and very small changes can translate to large positional deviations as the distance from the axis increases. However, three residues in the linker region show dramatic changes in Φ−Ψ torsions in the different structures (Figure 5A). These changes may be important for the hinge movement that causes the large-scale rigid-body motion of the lobes. In addition, torsional changes in the linker have a local influence, both on the shape and chemistry of the ATP-binding pocket. Most notable is the change in Φ of Gly250 and Ψ of Leu249. These rotations change the orientation of the carbonyl of Leu249. In molecule A of the apoenzyme and ADP structures, the carbonyl is inside the pocket pointing toward the large lobe; in the ATP-bound form, it points out of the pocket and down; in the AMP−PNP structure, it points into the pocket and up toward the nucleotide (Figure 5A). The conformation in the AMP−PNP structure pushes the adenine ring further away from the linker than it is in either the ATP or ADP structures.

To investigate whether flexibility of the linker is important for the function of Sky1p, we mutated Gly250 to Ala. This

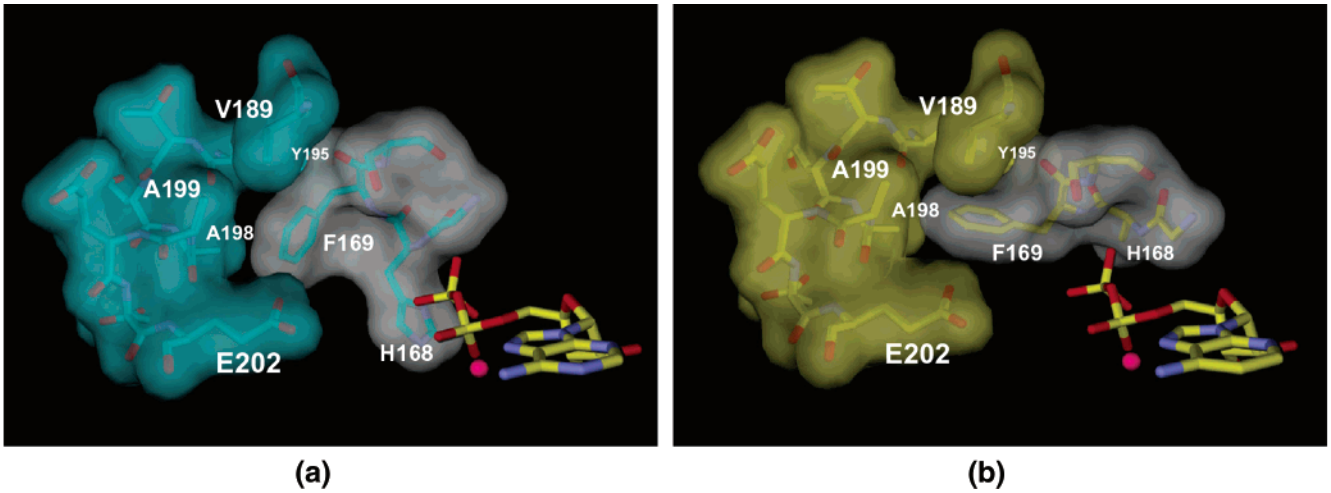

FIGURE 6: Conformation of the glycine-rich loop in the apoenzyme structure. (a) The glycine-rich loop adopts a twisted conformation in the apoenzyme structure. The face of Phe169 from the glycine-rich loop (gray surface) packs against a hydrophobic pocket formed by residues from helix αC and Val189 from β3 (cyan surfaces). In this conformation, the main chain of the tip of the loop twists inward, preventing backbone amides of the loop from hydrogen bonding to the phosphates of a bound nucleotide. In addition, the twist of the loop allows His168 to reach across the cleft, blocking the position that would be occupied by the γ phosphate of ATP. ADP and Mg2 (magenta sphere) from molecule A of the ADP-soaked crystals are depicted for comparison with (b). Note that Tyr95 is behind Val189 in the figure. This conformation of the loop may play a role in the release of ADP from the active site after phosphotransfer has occurred. (b) The glycine-rich loop adopts a flat and open conformation when nucleotide is bound. In the ADP-containing structure, Phe169 fills the hydrophobic pocket (yellow surfaces) with the face of the ring flat against Val189 from β3. Closing of the cleft relative to the apoenzyme structure causes a downward movement of Val189 and creates a tighter pocket. Phe169 changes rotomers to fill this tight pocket, and the loop untwists, making the backbone amides available for hydrogen bonding to the phosphates of a bound nucleotide. His168 exhibited poor density in this structure and is modeled as alanine.

mutant consistently showed a 2−3-fold reduced specific activity toward Npl3p (Figure 5B). This suggests that conformational flexibility dependent on the free rotation of the backbone of Gly250 is necessary for efficient substrate phosphorylation. In a previous study, we showed that Npl3p phosphorylation occurs rapidly in the active site and that substrate turnover is limited by net product release or associated conformational changes or both (*45*). Whether the mutational effect at position 250 is due to changes in the local environment of the ATP-binding pocket or to the slowing of lobe movements necessary for catalysis awaits further experimentation.

Conformation of the Glycine-Rich Loop in the Apoenzyme Structure. The glycine-rich loop twists inward toward helix αC in both molecules of the Sky1p apoenzyme structure, whereas it lies flat over the phosphates in the nucleotide-containing structures (Figure 6a and b). The aromatic ring of Phe169, a residue on the inside of the tip of the loop, changes rotamers to lie flat against a hydrophobic surface formed by Tyr195, Ala198, Ala199, and Glu202 from the C-helix and Val189 from β3. The rotamer change is accompanied by a twisting motion of the loop. In the ATP- and ADP-containing structures, movement of the small lobe pushes Val189 downward, tightening up this hydrophobic pocket. To fill the pocket, Phe169 slides in edgewise, butting the side of the ring against the C-helix, the face interacting with Val189. This interaction untwists the glycine-rich loop, and may provide a way for lobe closure and loop conformation to be coordinated. Although Phe169 is not conserved within the protein kinase family, the position is most often occupied by phenylalanine or tyrosine (*34*). Residues forming the surface that interacts with this phenylalanine, however, show a great deal of sequence and structural diversity among protein kinases.

His168, which is on the outside tip of the loop, reaches across the cleft and comes within hydrogen-bonding distance of Asp294, an essential residue for catalysis thought to be involved in either activating the nucleophile for phosphotransfer or isolating the productive rotamer of the P-site residue (*46*). In contrast to the ADP- and ATP-containing structures, the side chain of His168 shows good electron density in the apoenzyme structure. Although this position is most often occupied by a serine, alanine, or threonine in other protein kinases, His168 is conserved among the SRPKs.

Modeling ATP into the active site of the apoenzyme structure revealed that the twisted conformation of the glycine-rich loop is incompatible with ATP binding. The conformation tucks away the backbone amides of the glycine-rich loop so that they are unavailable to hydrogen bond to the phosphates (Figure 6A). In addition, His168 would sterically clash with the γ phosphate of ATP. The previously reported apoenzmye structure of Sky1p (1HOW) does not exhibit the twisted conformation of the glycine-rich loop. However, a sulfate of crystallization mimics the γ phosphate, binding underneath the tip of the loop and pushing it outward (*17*). An analysis of other active apoenzyme forms of protein kinase structures revealed two other kinases, ERK2 and CK1, that also adopt a twisted glycine-rich loop, suggesting that this conformation plays a general role in catalysis, possibly by initiating the release of ADP (*31*, *51*).

Conformation and Catalysis in the SRPK Family: Order of Binding and Processivity. Kinetic data on Sky1p indicates that AMP−PNP can bind to Sky1p in the absence or presence of Npl3p (*45*). If opening of the lobes is necessary for binding and release of the nucleotide, it follows that Sky1p must be able to open and close while Npl3p is bound. In support of this, the structures we present here suggest that it is binding of the nucleotide, rather than the protein substrate, that

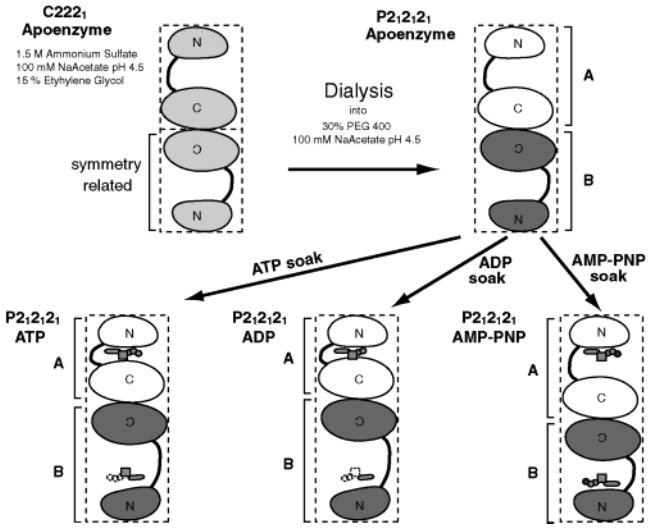

FIGURE 7: Schematic showing the effect of nucleotide binding on the asymmetric unit of the $P2_12_12_1$ structure. Soaking the $C222_1$ structure in PEG 400 and sodium acetate breaks a symmetry axis, creating the $P2_12_12_1$ packing arrangement. This arrangement has two molecules with slightly different conformations in an asymmetric unit (represented by the dotted line) that is twice as large as in the $C222_1$ crystals. When the $P2_12_12_1$ crystals are soaked with either ADP or ATP, the small lobe of molecule A rotates to close the cleft. This movement is accompanied by a compensating structural change in molecule B, in which the small lobe rotates in the opposite direction, opening the catalytic cleft. This compensatory movement allows the two molecules to make the same crystal contacts as those made in the apoenzyme $P2_12_12_1$ structure. Hence, the size of the asymmetric unit and the size of the unit cell are nearly identical, and large-scale conformational changes can occur without destroying the crystals. Electron density for the adenine ring of ADP and that of ATP were visible in molecule B, even though molecule B is forced into an open position. Mechanistic implications of this are discussed in the text. Soaking the $P2_12_12_1$ apoenzyme crystals in AMP−PNP causes almost no change in the relative orientation of the two lobes in either molecule A or molecule B, yet strong electron density is observed for the nucleotide in both active sites. This is due to differences in the chemistry of AMP−PNP versus ADP or ATP binding. These differences and their implications are discussed in the text.

induces closing and opening. However, the crystal structure of the Npl3p complexed to Sky1p in the presence and absence of nucleotide, or biophysical methods such as FRET which can probe the opening and closing of the kinase, are necessary to fully explore these issues.

CONCLUSIONS

We have presented four high-resolution structures of a single crystal form of Sky1p in different states of nucleotide binding. The $P2_12_12_1$ packing arrangement of these crystals is uniquely tolerant to conformational change, and by comparing equivalent molecules from the apoenzyme, AMP−PNP-, ADP-, and ATP-bound structures, we were able to monitor structural changes due solely to nucleotide binding (Figure 7). Both ADP and ATP binding induced lobe closure in molecule A of the asymmetric unit, with ADP causing slightly more closure than did ATP. In molecule B, crystal packing locks Sky1p into the open conformation, and only the adenine ring of ADP or ATP is ordered, suggesting that the first step in nucleotide binding involves adenine sticking to the roof at the back of the open cleft. A comparison of the contacts to the kinase made by the inhibitor AMP−PNP with those made by the reactant and product nucleotides has allowed us to determine which interactions are necessary for subsequent steps in closure. We also observed conformational changes in the glycine-rich loop that may provide a molecular basis for the ejection of ADP from the active site, which prepares Sky1p for the next round of catalysis. Finally, we have shown that a glycine in the linker between the lobes provides flexibility necessary for full kinase activity, either in shaping the back of the pocket or in facilitating lobe closure. These structures provide the basis for further biochemical experiments that will allow us to elucidate the role of conformational changes in the function of protein kinases.

ACKNOWLEDGMENT

We thank Brandon Aubol for helpful discussions and Nick Nguyen for help at the UCSD X-ray facility. We also acknowledge the W. M. Keck Laboratory for Integrated Biology II for providing computation time and Robert Konecny for his help at Keck II.

REFERENCES

1. Fu, X. D. (1995) *RNA 1*, 663−80.
2. Blencowe, B. J., Bowman, J. A., McCracken, S., and Rosonina, E. (1999) *Biochem. Cell Biol. 77*, 277−291.
3. Xiao, S. H., and Manley, J. L. (1997) *Genes Dev. 11*, 334−344.
4. Wang, H. Y., Lin, W., Dyck, J. A., Yeakley, J. M., Songyang, Z., Cantley, L. C., and Fu, X. D. (1998) *J. Cell Biol. 140*, 737−750.
5. Stojdl, D. F., and Bell, J. C. (1999) *Biochem. Cell Biol. 77*, 293−298.
6. Yeakley, J. M., Tronchere, H., Olesen, J., Dyck, J. A., Wang, H. Y., and Fu, X. D. (1999) *J. Cell Biol. 145*, 447−455.
7. Hartmann, A. M., Rujescu, D., Giannakouros, T., Nikolakaki, E., Goedert, M., Mandelkow, E. M., Gao, Q. S., Andreadis, A., and Stamm, S. (2001) *Mol. Cell. Neurosci. 18*, 80−90.
8. Gui, J. F., Tronchere, H., Chandler, S. D., and Fu, X. D. (1994) *Proc. Natl. Acad. Sci. U.S.A. 91*, 10824−10828.
9. Colwill, K., Feng, L. L., Yeakley, J. M., Gish, G. D., Caceres, J. F., Pawson, T., and Fu, X. D. (1996) *J. Biol. Chem. 271*, 24569−24575.
10. Nikolakaki, E., Meier, J., Simos, G., Georgatos, S. D., and Giannakouros, T. (1997) *J. Biol. Chem. 272*, 6208−6213.
11. Papoutsopoulou, S., Nikolakaki, E., Chalepakis, G., Kruft, V., Chevaillier, P., and Giannakouros, T. (1999) *Nucleic Acids Res. 27*, 2972−2980.
12. Daub, H., Blencke, S., Habenberger, P., Kurtenbach, A., Dennenmoser, J., Wissing, J., Ullrich, A., and Cotten, M. (2002) *J. Virol. 76*, 8124−8137.
13. Tang, Z., Yanagida, M., and Lin, R. J. (1998) *J. Biol. Chem. 273*, 5963−5969.
14. Erez, O., and Kahana, C. (2001) *Mol. Cell. Biol. 21*, 175−184.
15. Sanz, G., Mir, L., and Jacquemin-Sablon, A. (2002) *Cancer Res. 62*, 4453−4458.
16. Schenk, P. W., Boersma, A. W., Brok, M., Burger, H., Stoter, G., and Nooter, K. (2002) *Mol. Pharmacol. 61*, 659−666.
17. Nolen, B., Yun, C. Y., Wong, C. F., McCammon, J. A., Fu, X. D., and Ghosh, G. (2001) *Nat. Struct. Biol. 8*, 176−183.
18. Sowadski, J. M., Epstein, L. F., Lankiewicz, L., and Karlsson, R. (1999) *Pharmacol. Ther. 82*, 157−164.
19. Zheng, J., Knighton, D. R., Xuong, N. H., Taylor, S. S., Sowadski, J. M., and Ten Eyck, L. F. (1993) *Protein Sci. 2*, 1559−1573.
20. Shaffer, J., and Adams, J. A. (1999) *Biochemistry 38*, 5572−5581.
21. Shaffer, J., and Adams, J. A. (1999) *Biochemistry 38*, 12072−12079.
22. Jan, A. Y., Johnson, E. F., Diamonti, A. J., Carraway, I. K., and Anderson, K. S. (2000) *Biochemistry 39*, 9786−9803.
23. Shaffer, J., Sun, G., and Adams, J. A. (2001) *Biochemistry 40*, 11149−11155.

24. Andersen, M. D., Shaffer, J., Jennings, P. A., and Adams, J. A. (2001) *J. Biol. Chem. 276*, 14204−14211.
25. Hamuro, Y., Wong, L., Shaffer, J., Kim, J. S., Stranz, D. D., Jennings, P. A., Woods, V. L., Jr., and Adams, J. A. (2002) *J. Mol. Biol. 323*, 871−881.
26. Li, F., Gangal, M., Juliano, C., Gorfain, E., Taylor, S. S., and Johnson, D. A. (2002) *J. Mol. Biol. 315*, 459−469.
27. Ogawa, A., Takayama, Y., Sakai, H., Chong, K. T., Takeuchi, S., Nakagawa, A., Nada, S., Okada, M., and Tsukihara, T. (2002) *J. Biol. Chem. 277*, 14351−14354.
28. Gill, S. C., and von Hippel, P. H. (1989) *Anal. Biochem. 182*, 319−326.
29. Brunger, A. T., Adams, P. D., Clore, G. M., DeLano, W. L., Gros, P., Grosse-Kunstleve, R. W., Jiang, J. S., Kuszewski, J., Nilges, M., Pannu, N. S., Read, R. J., Rice, L. M., Simonson, T., and Warren, G. L. (1998) *Acta Crystallogr., Sect. D 54 (Pt 5)*, 905−921.
30. Xu, R. M., Carmel, G., Sweet, R. M., Kuret, J., and Cheng, X. (1995) *EMBO J. 14*, 1015−1023.
31. Longenecker, K. L., Roach, P. J., and Hurley, T. D. (1996) *J. Mol. Biol. 257*, 618−631.
32. Lowe, E. D., Noble, M. E., Skamnaki, V. T., Oikonomakos, N. G., Owen, D. J., and Johnson, L. N. (1997) *EMBO J. 16*, 6646−6658.
33. Zheng, J., Knighton, D. R., Ten Eyck, L. F., Karlsson, R., Xuong, N., Taylor, S. S., and Sowadski, J. M. (1993) *Biochemistry 32*, 2154−2161.
34. Buzko, O., and Shokat, K. M. (2002) *Bioinformatics 18*, 1274−1275.
35. Batkin, M., and Shaltiel, S. (1999) *FEBS Lett. 452*, 395−399.
36. Brown, N. R., Noble, M. E., Endicott, J. A., and Johnson, L. N. (1999) *Nat. Cell Biol. 1*, 438−443.
37. Favelyukis, S., Till, J. H., Hubbard, S. R., and Miller, W. T. (2001) *Nat. Struct. Biol. 8*, 1058−1063.
38. Cook, A., Lowe, E. D., Chrysina, E. D., Skamnaki, V. T., Oikonomakos, N. G., and Johnson, L. N. (2002) *Biochemistry 41*, 7301−7311.
39. Madhusudan, P. A., Xuong, N.-H., and Taylor, S. S. (2002) *Nat. Struct. Biol. 9*, 273−277.
40. Smith, C. M., Radzio-Andzelm, E., Madhusudan, P. A., and Taylor, S. S. (1999) *Prog. Biophys. Mol. Biol. 71*, 313−341.
41. Taylor, S. S., Knighton, D. R., Zheng, J., Ten Eyck, L. F., and Sowadski, J. M. (1992) *Annu. Rev. Cell Biol. 8*, 429−462.
42. Aimes, R. T., Hemmer, W., and Taylor, S. S. (2000) *Biochemistry 39*, 8325−8332.
43. Grant, B. D., Hemmer, W., Tsigelny, I., Adams, J. A., and Taylor, S. S. (1998) *Biochemistry 37*, 7708−7715.
44. Russo, A. A., Jeffrey, P. D., and Pavletich, N. P. (1996) *Nat. Struct. Biol. 3*, 696−700.
45. Aubol, B. E., Nolen, B., Vu, D., Ghosh, G., and Adams, J. A. (2002) *Biochemistry 41*, 10002−10009.
46. Adams, J. A. (2001) *Chem. Rev. 101*, 2271−2290.
47. Madhusudan, E. A. Trafny, Xuong, N. H., Adams, J. A., Ten Eyck, L. F., Taylor, S. S., and Sowadski, J. M. (1994) *Protein Sci. 3*, 176−187.
48. Niefind, K., Guerra, B., Pinna, L. A., Issinger, O. G., and Schomburg, D. (1998) *EMBO J. 17*, 2451−2462.
49. Hutter, M. C., and Helms, V. (1999) *Protein Sci. 8*, 2728−2733.
50. Gibbs, C. S., and Zoller, M. J. (1991) *J. Biol. Chem. 266*, 8923−8931.
51. Canagarajah, B. J., Khokhlatchev, A., Cobb, M. H., and Goldsmith, E. J. (1997) *Cell 90*, 859−869.
52. McRee, D. E., and David, P. R. (1999) *Practical Protein Crystallography*, 2nd ed., Academic Press, San Diego, CA.
53. Merritt, E. A., and Bacon, D. J. (1997) *Methods Enzymol. 277*, 505−524.
54. Jones, T. A., Zou, J. Y., Cowan, S. W., and Kjeldgaard. (1991) *Acta Crystallogr., Sect. A 47* (Pt 2), 110−119.
55. Hayward, S., and Berendsen, H. J. (1998) *Proteins: Struct., Funct., Genet. 30*, 144−154.
56. Kraulis, P. J. (1991) *J. Appl. Crystallogr. 24*, 946−950.

BI0344331